



**HAL**  
open science

## Two-fluid numerical simulations of turbulence inside Kelvin-Helmholtz vortices: Intermittency and reconnecting current sheets

C. Rossi, F. Califano, Alessandro Retinò, L. Sorriso-Valvo, Pierre Henri, S. Servidio, F. Valentini, A. Chasapis, Laurence Rezeau

### ► To cite this version:

C. Rossi, F. Califano, Alessandro Retinò, L. Sorriso-Valvo, Pierre Henri, et al.. Two-fluid numerical simulations of turbulence inside Kelvin-Helmholtz vortices: Intermittency and reconnecting current sheets. *Physics of Plasmas*, 2015, 22 (12), pp.122303. 10.1063/1.4936795 . insu-01352156

**HAL Id: insu-01352156**

**<https://insu.hal.science/insu-01352156>**

Submitted on 25 Sep 2020

**HAL** is a multi-disciplinary open access archive for the deposit and dissemination of scientific research documents, whether they are published or not. The documents may come from teaching and research institutions in France or abroad, or from public or private research centers.

L'archive ouverte pluridisciplinaire **HAL**, est destinée au dépôt et à la diffusion de documents scientifiques de niveau recherche, publiés ou non, émanant des établissements d'enseignement et de recherche français ou étrangers, des laboratoires publics ou privés.

## Two-fluid numerical simulations of turbulence inside Kelvin-Helmholtz vortices: Intermittency and reconnecting current sheets

C. Rossi, F. Califano, A. Retinò, L. Sorriso-Valvo, P. Henri, S. Servidio, F. Valentini, A. Chasapis, and L. Rezeau

Citation: *Physics of Plasmas* **22**, 122303 (2015); doi: 10.1063/1.4936795

View online: <http://dx.doi.org/10.1063/1.4936795>

View Table of Contents: <http://scitation.aip.org/content/aip/journal/pop/22/12?ver=pdfcov>

Published by the [AIP Publishing](#)

---

### Articles you may be interested in

[Evolution of electron current sheets in collisionless magnetic reconnection](#)

*Phys. Plasmas* **22**, 102110 (2015); 10.1063/1.4933120

[Evolution of the magnetic field generated by the Kelvin-Helmholtz instability](#)

*Phys. Plasmas* **21**, 072126 (2014); 10.1063/1.4891340

[Nonlinear evolution of the magnetized Kelvin-Helmholtz instability: From fluid to kinetic modeling](#)

*Phys. Plasmas* **20**, 102118 (2013); 10.1063/1.4826214

[Kelvin-Helmholtz instability in a current-vortex sheet at a 3D magnetic null](#)

*Phys. Plasmas* **20**, 032117 (2013); 10.1063/1.4798516

[Magnetised Kelvin-Helmholtz instability in the intermediate regime between subsonic and supersonic regimes](#)

*Phys. Plasmas* **19**, 072908 (2012); 10.1063/1.4739234

---



**PFEIFFER VACUUM**

## VACUUM SOLUTIONS FROM A SINGLE SOURCE

Pfeiffer Vacuum stands for innovative and custom vacuum solutions worldwide, technological perfection, competent advice and reliable service.

**125 YEARS**  
NOTHING IS BETTER

## Two-fluid numerical simulations of turbulence inside Kelvin-Helmholtz vortices: Intermittency and reconnecting current sheets

C. Rossi,<sup>1,2,a)</sup> F. Califano,<sup>1</sup> A. Retinò,<sup>2</sup> L. Sorriso-Valvo,<sup>3</sup> P. Henri,<sup>4</sup> S. Servidio,<sup>5</sup> F. Valentini,<sup>5</sup> A. Chasapis,<sup>2</sup> and L. Rezeau<sup>2</sup>

<sup>1</sup>*Dip. Fisica, Università di Pisa, Largo Pontecorvo 3, 56127 Pisa, Italy*

<sup>2</sup>*LPP-CNRS/École Polytechnique/UPMC/Université Paris Sud, 91128 Palaiseau Cedex, France*

<sup>3</sup>*Nanotec-CNR, U.O.S. LICRYL di Cosenza, Ponte P. Bucci, Cubo 31C, I-87036 Rende, Italy*

<sup>4</sup>*LPC2E, CNRS, Orléans, France*

<sup>5</sup>*Dipartimento di Fisica, Università della Calabria, I-87036 Rende, CS, Italy*

(Received 13 June 2015; accepted 12 November 2015; published online 9 December 2015)

The turbulence developing inside Kelvin-Helmholtz vortices has been studied using a two-fluid numerical simulation. From an initial large-scale velocity shear, the nonlinear evolution of the instability leads to the formation of a region inside the initial vortex characterized by small-scale fluctuations and structures. The magnetic energy spectrum is compatible with a Kolmogorov-like power-law decay, followed by a steeper power-law below proton scales, in agreement with other studies. The magnetic field increments show non-Gaussian distributions with increasing tails going towards smaller scales, consistent with presence of intermittency. The strong magnetic field fluctuations populating the tails of the distributions have been identified as current sheets by using the Partial Variance of the Increments (PVI) method. The strongest current sheets (largest PVI) appear around proton scales and below. By selecting several of such current sheets, it has been found that most of them are consistent with ongoing magnetic reconnection. The detailed study of one reconnecting current sheet as crossed by a virtual spacecraft is also presented. Inflow and outflow regions have been identified and the reconnection rate has been estimated. The observation of reconnection rates higher than typical fast rate  $\sim 0.1$  suggests that reconnection in turbulent plasma can be faster than laminar reconnection. This study indicates that intermittency and reconnecting current sheets are important ingredients of turbulence within Kelvin-Helmholtz vortices and that reconnection can play an important role for energy dissipation therein. © 2015 AIP Publishing LLC.

[<http://dx.doi.org/10.1063/1.4936795>]

### I. INTRODUCTION

Turbulence is a universal phenomenon occurring in fluids as well as in magnetized collisionless plasma, as, e.g., in the near-Earth's environment,<sup>1</sup> in planets' magnetosphere,<sup>2</sup> and in the solar wind.<sup>3,4</sup> In this work, we focus on the spontaneous development of turbulence in the saturated phase of the Kelvin-Helmholtz (K-H) instability.<sup>5,6</sup> The physical reference is the low latitude Earth's magnetosphere<sup>7</sup> where the shear flow between solar wind and magnetosphere plasmas provides the conditions for this instability to develop and to create a chain of large scale vortices. The development of the K-H instability is particularly important in terms of solar wind plasma transport into the Earth's magnetosphere.<sup>8–11</sup> During the evolution of the instability, the vortices evolve nonlinearly and interact one with each other leading to merging or being disrupted. The vortices disruption is driven by the development of secondary instabilities<sup>12</sup> around the edge of the arms of the vortices, in between or inside the vortices themselves. The evolution is thus characterized by a rich non-linear dynamics leading to the formation of a mixing layer where the magnetospheric and solar wind plasma interact. Spacecraft observations show the presence of this broad boundary layer during northward orientation of the interplanetary magnetic

field,<sup>13</sup> and vortices have been detected at the low latitude magnetopause.<sup>9,14</sup> Here, we study the small scale dynamics and structures occurring inside the mixing layer and analyse the turbulent behaviour by using a two-fluid, 2.5D numerical simulations.<sup>15</sup>

Fluid simulations remain at today a fundamental tool to explore the turbulent motions driven by the energy typically injected at the very large-scales. The main motivation is the possibility to include several decades up to the ion range, but starting from the MHD scales, thus correctly reproducing the mechanisms of the energy transfer towards, and injection into, the kinetic part. The price to be paid is the loss of the kinetic part of the physics at small-scales; in this sense, fluid simulations are complementary to kinetic simulations. In this context, our aim here is to explore the goodness and the limits of the (two)-fluid models in capturing the main physics when crossing the kinetic ion scales such as the ion Larmor radius and ion inertial length eventually ending in a fully turbulent state. This transition is naturally achieved by the evolution of the K-H instability and recently studied also by means of kinetic simulations.<sup>5,6</sup> In particular, Henri *et al.*<sup>16</sup> in studying K-H instability have compared Hybrid PIC simulations with those obtained from fluid models, showing that the two-fluid model reasonably reproduced the main dynamics of the long time non-linear evolution of the K-H instability. We underline that the possibility of using fluid models in

<sup>a)</sup>claudia.rossi@df.unipi.it

certain regimes represents an important step forward in order to reduce the computational requirements of full kinetic simulations, also in the perspective of providing an alternative tool for the interpretation of experimental data.

In Section II, we present the numerical code used for the simulations; in Section III, we analyse the properties of turbulence, such as the spectrum and the anisotropy of the system; in Section IV, we study intermittency of the structures in this system; finally in Section VI, we studied in detail one of such structures as a typical magnetic reconnection site.

## II. THE TWO FLUID CODE

The two-dimensional numerical code integrates the Hall-MHD system of equations using dimensionless variables obtained normalizing to ion characteristic quantities, the ion mass  $m_i$ , the Alfvén velocity  $V_A$ , and the ion inertial length  $d_i$ . The continuity and motion equations read

$$\frac{\partial n}{\partial t} + \nabla \cdot (n\mathbf{u}_i) = 0, \quad (1)$$

$$\frac{\partial(n\mathbf{u}_i)}{\partial t} + \nabla \cdot [n(\mathbf{u}_i\mathbf{u}_i + P_{tot}\mathbf{I} - \mathbf{B}\mathbf{B})] = 0, \quad (2)$$

where  $\mathbf{u}_i$  is the ion velocity,  $n$  is the density,  $\mathbf{B}$  is the total magnetic field, and  $P_{tot}\mathbf{I}$  is the pressure tensor. We assume isotropic, scalar pressures, so that  $\mathbf{I}$  is the identity matrix and  $P_{tot}$  is the total pressure, defined as  $P_{tot} = P_e + P_i + B^2/2$ . The subscripts  $e, i$  indicate the electrons and the ions, respectively. Quasi neutrality is assumed,  $n_i \sim n_e \sim n$ , and the displacement current is neglected. Adiabatic closures are used for both electrons and ions

$$\frac{\partial(nS_{e,i})}{\partial t} + \nabla \cdot (nS_{e,i}\mathbf{u}_{e,i}) = 0, \quad (3)$$

where  $S_{e,i} = P_{e,i}n^{-\gamma}$ ,  $\gamma = 5/3$  is the polytropic index, and  $u_e$  and  $u_i$  are the electron and ion velocities, respectively. The electric field is calculated through the generalized Ohm's law

$$\mathbf{E} = -\mathbf{u}_e \times \mathbf{B} - \frac{1}{n}\nabla P_e. \quad (4)$$

The magnetic field is calculated using the Faraday equation. The code uses a third order Runge-Kutta scheme for temporal discretization and a compact finite difference scheme with spectral-like resolution for spatial derivatives along the inhomogeneous  $x$ -direction. Numerical stability is achieved through the use of numerical filters.<sup>17</sup> The simulation has periodic boundary conditions in the  $y$ -direction (direction of the solar wind flow) and open boundary transparent conditions in the  $x$ -direction.<sup>15</sup> A spectral filter is used along the periodic  $y$ -direction and a sixth order spectral like filtering scheme along the inhomogeneous  $x$ -direction. Here the filters are used to smooth out only the very short scale-lengths of the system.

The code convergence has been checked by changing the grid resolution not only to study the KH instability evolution but also to test the code correctness on several different

linear instabilities and/or non-linear dynamics. Moreover, during the simulation, we check the average value of  $|\nabla(B)|/|B|$  which remains less than  $10^{-7}$  and, most important, which do not show any exponential growth in time. We underline that both the in-plane magnetic energy and the ion thermal energy increase in time of the order of several percent at the expense of the ion kinetic energy (in this model electrons are assumed as massless).

## A. Initial setup

A large scale initial velocity shear along the  $y$ -direction and a mostly out-of-plane magnetic field are used to initialize the simulation

$$u_{iy}(x) = u_{ey}(x) = A_{eq} \tanh\left(\frac{x - L_x/2}{L_{eq}}\right), \quad (5)$$

$$\mathbf{B}(x) = (0, B_0 \sin \vartheta, B_0 \cos \vartheta), \quad (6)$$

with  $B_0 = 1$ ,  $A_{eq} = 1$ ,  $L_{eq} = 6$ , and  $\vartheta = 0.02$  rad. Furthermore, we take a constant initial density and temperature,  $n = 1.0$ , and  $T_i = T_e = 0.5$ . The numerical domain is given by  $L_x \times L_y = [400 \times 402] d_i$  with resolution  $dx = 0.1 d_i$  and  $dy = 0.05 d_i$ , corresponding to  $N_x \times N_y = 4096 \times 8192$  grid points.

## III. NON-LINEAR TURBULENT EVOLUTION

The primary Kelvin-Helmholtz instability and its further dynamics are characterized by three main phases: the linear phase, when the instability develops; the non-linear phase, with the formation of the characteristic vortices interacting with each other; and the saturated phase, when the vortices have evolved. During the non-linear phase, the development of secondary instabilities drives the formation of small scale fluctuations and structures, of the order of one inertial length or less. This is shown in Fig. 1 where we draw the shaded iso-contours of the  $J_z(x, y)$  component in the  $(x, y)$ -plane at the end of the saturated phase ( $t = 1000 \Omega_{ci}^{-1}$ ), together with the magnetic potential field lines. Since we are interested in studying the turbulent dynamics during the saturated phase,

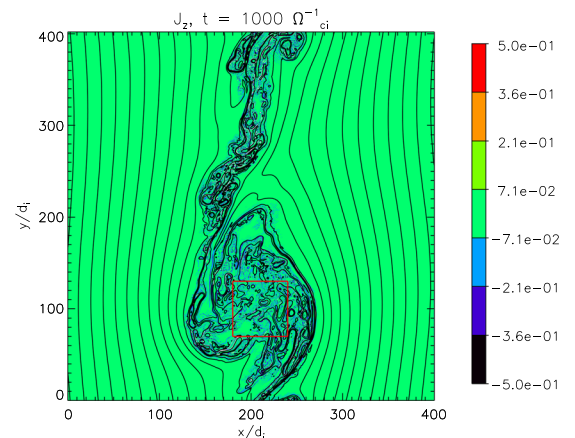


FIG. 1. Shaded iso-contours of the out-of plane current  $J_z(x, y)$  together with magnetic potential field lines. The red square box delimits a turbulent region inside the K-H vortex.

we select a square box in the turbulent area as shown in Fig. 1. A zoom of the box marked in red is shown in Fig. 2. It contains the iso-contours of the out-of-plane current  $J_z$ , with over-plotted the magnetic potential lines in the domain  $[180 - 240] d_i \times [70 - 130] d_i$ . This figure clearly shows a turbulent dynamics characterized by the presence of small scale structures and by strong current fluctuations. This is the largest square box we can take inside the turbulent region, selected in order to avoid the influence of the vortex ribbons (outer scale structures). In this box, we have calculated the energy spectra of the magnetic field fluctuations, defined as  $\delta B_i(x, y) = B_i(x, y) - \langle B_i(x, y) \rangle$ ,  $i = x, y, z$ , and calculated the total spectral magnetic energy of the fluctuations. In order to estimate the power spectrum of the fluctuations, we have applied a 2D Fourier transform combined with a Hanning window, chosen because side lobes fall off rapidly in this window. By analysing the evolution of the distribution of the spectral magnetic energy in the wave-vector space  $(k_x, k_y)$ , we observe that the system was initially strongly anisotropic, due to the velocity shear imposed in the  $x$ -direction and due to the fact that the vortex structures are not round shaped. A weaker anisotropy is also introduced by the in-plane component of the mean magnetic field. However, as expected, this anisotropy is progressively destroyed during the non-linear dynamics of the system. The level of isotropy of a system can be quantified using the Shebalin angle,<sup>18</sup> this quantity measures the ratio between the energy in the perpendicular direction and in the parallel direction, with respect to the magnetic field, and it is defined as

$$\tan^2 \vartheta_B = \frac{\sum_k k_x^2 |\delta \mathbf{B}(k_x, k_y)|^2}{\sum_k k_y^2 |\delta \mathbf{B}(k_x, k_y)|^2}. \quad (7)$$

For an isotropic spectrum, one gets  $\vartheta = 45^\circ$ , corresponding to  $\tan^2 \vartheta = 1$ . A tendency to an isotropic value is observed by calculating  $\tan^2 \vartheta$  throughout the simulation. During the linear phase of the primary K-H, its value is of the order of  $\tan^2 \vartheta = 4$ , corresponding to  $\vartheta \sim 63^\circ$ . However, as soon as the vortex non-linear dynamics take place, secondary instabilities develop and the Shebalin angle value is decreased

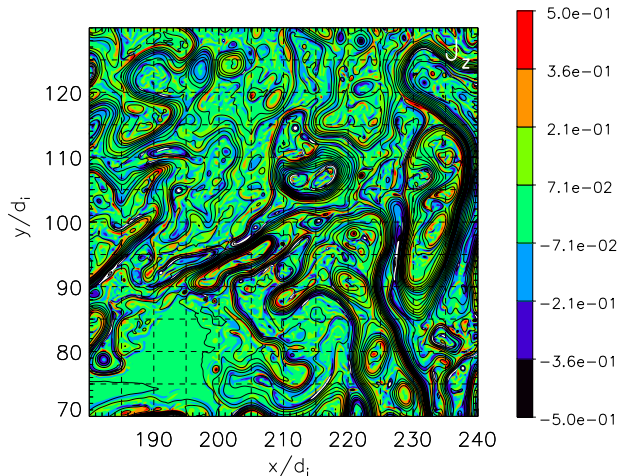


FIG. 2. Magnification of out-of-plane current in the red box indicated in Fig. 1 in the domain  $[180 - 240] d_i \times [70 - 130] d_i$ .

more and more until it reaches the isotropic value  $\tan \vartheta \sim 1$  in the final phase of the simulation,  $t \sim 1000 \Omega_{ci}^{-1}$ .

Once the isotropic spectral configuration has been achieved, we calculate the magnetic spectrum by integrating the energy of magnetic fluctuations over concentric shells from  $k_{min} = 2\pi/L_x = 0.1 d_i^{-1}$  to  $k_{max} = 2\pi/(2dx) = 32 d_i^{-1}$ . The results are shown in the omni-directional spectrum given in Fig. 3. The dashed turquoise part of the spectrum indicates the scales where the filters are effective, resulting in an exponential decay. The injection scale (vertical dashed line in Fig. 3),  $k_{inj} d_i = 0.04$ , corresponds to the most unstable wave vector of the primary K-H instability, and its corresponding wavelength to the initial vortex size. At smaller scales  $0.2 < k_\perp d_i < 1$ , i.e., in the MHD range, the spectrum is well represented by a power law with an exponent  $-1.8$  (continuous red line in Fig. 3), not far from the Kolmogorov value  $5/3$ . This observation is consistent with particle-in-cell simulations of K-H turbulence.<sup>6</sup> This behaviour is observed starting from  $t \simeq 750 \Omega_{ci}^{-1}$ , corresponding to the onset of the saturated phase. It is worth noticing that our model has been chosen to study the dynamics around the proton scales, so that we do not expect to observe an extended inertial range. However, a break in the power-law spectrum is present around  $k_\perp d_i \sim 1$ . Below proton scales, the spectrum is compatible with a steeper power law  $\simeq k_\perp^{-3.8}$  (continuous blue line in Fig. 3). Such exponent is somewhat larger than the one found in the same range in particle-in-cell simulations,<sup>5</sup> and it is within the values typically observed in near-Earth space.<sup>19-22</sup>

#### IV. INCREMENTS AND PROBABILITY DISTRIBUTION FUNCTION (PDF)

To characterize the turbulence inside the K-H vortex, we have studied the PDFs of the magnetic field increments, which is defined as

$$\Delta \mathbf{B}(\mathbf{r}, \mathbf{l}) = \mathbf{B}(\mathbf{r} + \mathbf{l}) - \mathbf{B}(\mathbf{r}), \quad (8)$$

where  $\mathbf{r} = (x, y)$  is the position and  $\mathbf{l} = (l_x, l_y)$  is the scale vector. For each component of the magnetic field, increments have been evaluated in the  $x$ - and  $y$ -directions, in the range

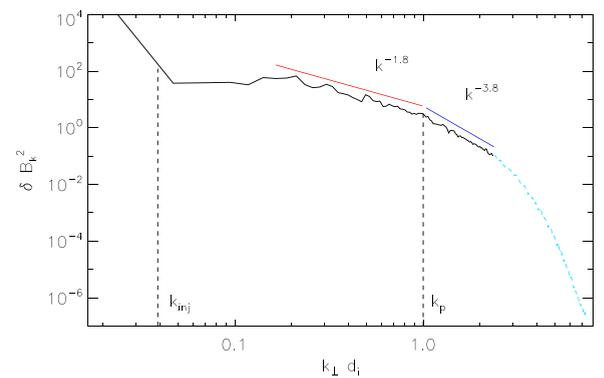


FIG. 3. Omnidirectional magnetic energy spectra, obtained by integrating over concentric shells in the  $(k_x, k_y)$  wave-vector space. A Kolmogorov-like spectrum is observed at MHD scales, while a steeper power law is suggested below proton scales. The spectrum at scales  $k_\perp d_i > 3$  is dominated by the action of the numerical filters in the simulations.

of scales  $1.5 d_i \leq |l| \leq 20 d_i$ . In Fig. 4, top panel, we show the PDFs of the increments of the  $B_x$  component calculated inside the red box of Fig. 1, for ten different scales. For each scale, the magnetic field increments were standardized by normalizing to their standard deviation. The blue dashed line represents a reference Gaussian distribution with  $\sigma = 1$ . Similar results were found for the  $B_y$  component (not shown here), confirming the isotropic nature of turbulence in this phase, in agreement with the Shebalin angle results.

First of all, we note that the probability distribution functions are characterized by high tails and that the deviation from Gaussian increases towards smaller scales. The scale dependence of the statistical properties of the field is usually referred to as intermittency and is universally observed in turbulent flows.<sup>23–25</sup> The fat tails are due to particularly intense magnetic field fluctuations, usually related to the presence of structures. Fat-tail PDFs of the magnetic field increments have been also found in PIC simulations of turbulence induced by a shear velocity field.<sup>5,6</sup>

For comparison, we have calculated the PDFs of the increments in a box selected outside the K-H vortex (not shown here). In this case, PDFs show a Gaussian behavior and typical of random motions where turbulence is not yet developed. Note that small scale Gaussian fluctuations are also observed in PIC simulations of turbulence.<sup>26</sup>

A different way to quantify the deviation from a Gaussian distribution is the flatness, which is defined as the normalized fourth order moment of increments

$$F(l) = \frac{\langle \Delta B(l)^4 \rangle}{\langle \Delta B(l)^2 \rangle^2}. \quad (9)$$

The flatness is significantly larger than the value expected for a Gaussian distribution  $F(l) = 3$  (Fig. 4, bottom panel). In particular, it increases from  $F(l) \sim 4$  at larger scales to  $F(l) \sim 9$  at smaller scales. This behaviour is quantitatively in

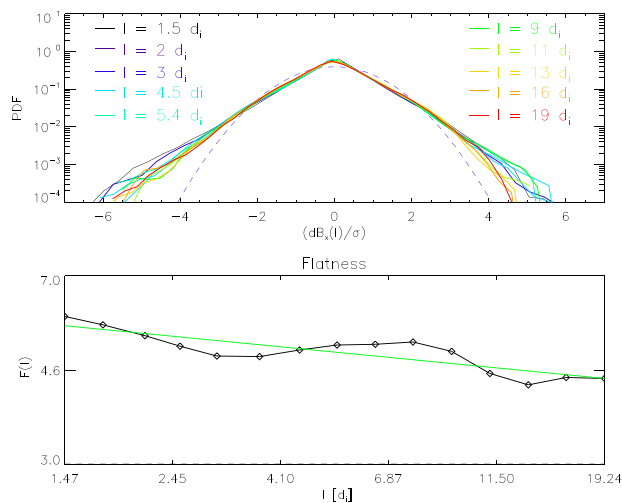


FIG. 4. The distribution functions of normalized increments  $\Delta B_x(l)$  are shown in the top panel of the box inside the K-H vortex. The blue dotted line is a Gaussian distribution used as reference. In the bottom panel, the Log-log plot of the flatness is plotted as a function of the scale; the value expected for a Gaussian distribution  $F = 3$  corresponds to the horizontal axis and the green superimposed line is a power-law fit.

agreement with the results found at ion scales in PIC simulations.<sup>5</sup>

It is interesting to note that the flatness increases as a power law of the scale,  $F(l) \sim l^{-\gamma}$ . The scaling exponent  $\gamma$  gives a quantitative estimate of the intermittency, i.e., of the anomalous scaling of the magnetic fluctuations.<sup>27</sup> A power-law fit of the flatness gives  $\gamma = 0.10 \pm 0.02$ , which is the typical value observed in Navier-Stokes turbulence.<sup>28</sup>

## V. RECONNECTION REGIONS

As we have mentioned in Sec. IV, intermittency is the signature of the increasing presence of relatively intense magnetic field fluctuations occurring towards small scales. In order to identify and characterize these structures, we have used the Partial Variance of the Increments (PVI),<sup>29,30</sup> which is defined as

$$PVI_i(l) = \frac{|\Delta B_i(l)|}{\sqrt{\langle |\Delta B_i(l)|^2 \rangle}}, \quad (10)$$

where  $i = x, y$  and the normalization factor is the standard deviation  $\sigma$  of the fluctuations at a given scale.

This quantity has been calculated at four different scales ( $l = 0.5, 1, 2, 5 d_i$ ) on vertical and horizontal cuts of the turbulent box in Fig. 2, separated by  $5 d_i$  and shown by dashed black lines. For each scale, we show in Fig. 5 the histograms of the number of structures with PVI intensity larger than  $\sigma$ ,  $2\sigma$ , and  $3\sigma$ , represented in blue, red, and yellow color, respectively.

The most intense structures with  $PVI > 3\sigma$  appear mostly at scales of the order of the ion inertial length,  $l = 0.5 - 1 d_i$ . High PVI structures are usually associated with reconnecting current sheets as revealed by the analysis of magnetic topology<sup>29,30</sup> and are important sites of energy dissipation, as shown by *in-situ* spacecraft observations.<sup>31–33</sup> Dissipation in thin current sheets has been specifically studied in 2D PIC simulations of shear-flow turbulence,<sup>5,6,26</sup> where the largest contribution to dissipation was found to be very intermittent and concentrated in small-scale current sheets with high values of the current density  $\mathbf{J}$ .<sup>5,26</sup> The dissipation in such simulations was quantified by evaluating the quantity  $\mathbf{E} \cdot \mathbf{J}$ . The formation of secondary islands was also found<sup>6</sup> which provides evidence of reconnection. In our

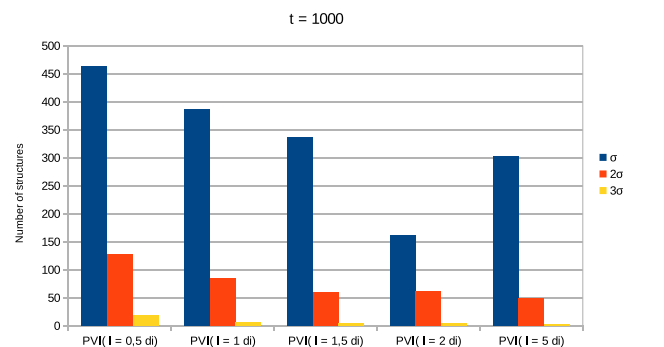


FIG. 5. Histograms of the total number of structures with PVI larger than  $\sigma$ ,  $2\sigma$ , and  $3\sigma$ , represented with blue, red, and yellow histograms, respectively. PVI was calculated for four scales,  $l = 0.5, 1, 2, 5 d_i$ .

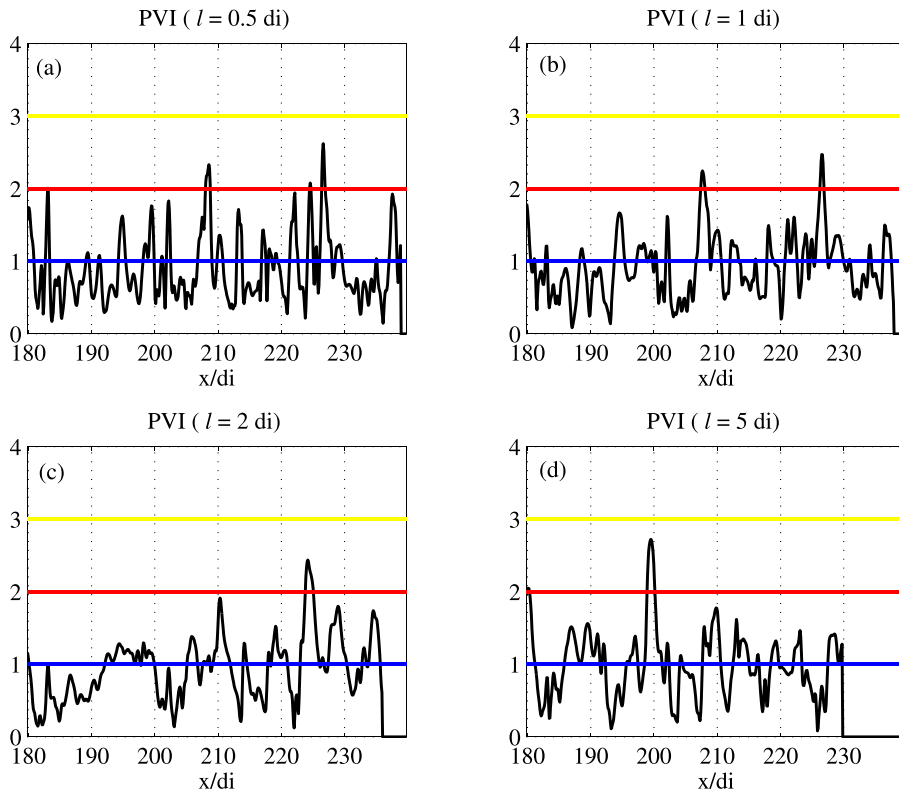


FIG. 6. Magnetic field PVI for the horizontal cut performed at  $y = 90 d_i$ . Top panels refer to scales  $l = 0.5 d_i$  and  $l = 1 d_i$  (top-left and top-right, respectively) and bottom panels to scales  $2 d_i$  and  $5 d_i$  (bottom-left and bottom-right panels, respectively). The thresholds are marked with horizontal continuous lines colored in blue for  $1\sigma$ , in red for  $2\sigma$ , and in yellow for  $3\sigma$ .

study, we provide evidence of reconnection by directly showing the expected reconnection signatures around the X-point (inflow/outflow patterns, Hall physics, etc.) as discussed in detail below. We have also observed the formation of islands (not shown), further supporting the reconnection scenario.

We have selected several structures characterized by large values of the PVI index (corresponding to large current densities), and we have checked their consistency with reconnecting current sheets by using a diagnostic similar to that used in spacecraft data analysis.<sup>31,32,34</sup> This diagnostic

complements the evidence of reconnection based on the analysis of the magnetic topology typically done in simulations of reconnection in turbulence.<sup>30,35</sup> As an example, in Fig. 6 we show the PVI computed at scales  $l = 0.5, 1, 2, 5 d_i$  for a cut along  $y = 90 d_i$  in Fig. 2. For this cut, we observe that the most intense current sheets have PVI larger than  $2\sigma$ . We selected one such current sheet having scale of the order of  $d_i$  ( $x \simeq 225$  in Fig. 6(b)). Note that the lag over which the PVI is calculated roughly identifies the thickness of the current sheets, as can be easily verified by visual inspection of the simulation data. Therefore, the histogram shown in Fig. 5 also roughly represents the distribution of the current sheet thickness.

Fig. 7 shows the magnetic field lines superposed to the out-of-plane current  $J_z$  for the selected current sheet. The local magnetic topology is compatible with a reconnection site. The dashed red lines mark the position of the X-point. There is a small density and magnetic field amplitude asymmetry across the current sheet (Table I), while the out-of-plane magnetic field  $B_z$  (guide field) is large with respect to the reconnecting component  $B_y$ ,  $B_z/B_y \simeq 5$ .

TABLE I. Main parameters in the two inflow regions R-I and R-II and in the outflow region for the selected current sheet. The two regions are defined in the ranges  $[226.5 - 226.75] d_i$  and  $[227.6 - 228] d_i$  along the x-axis.

	Inflow (R-I)	Outflow	Inflow (R-II)
$\langle B \rangle$	0.69	0.66	0.61
$\langle B_x \rangle$	0.03	0.02	0.02
$\langle B_y \rangle$	0.08	0.08	0.02
$\langle U_{e,x} \rangle$	0.06	0.01	0.03
$\langle U_{e,y} \rangle$	0.21	0.32	0.19
$\langle N \rangle$	0.6	0.63	0.66

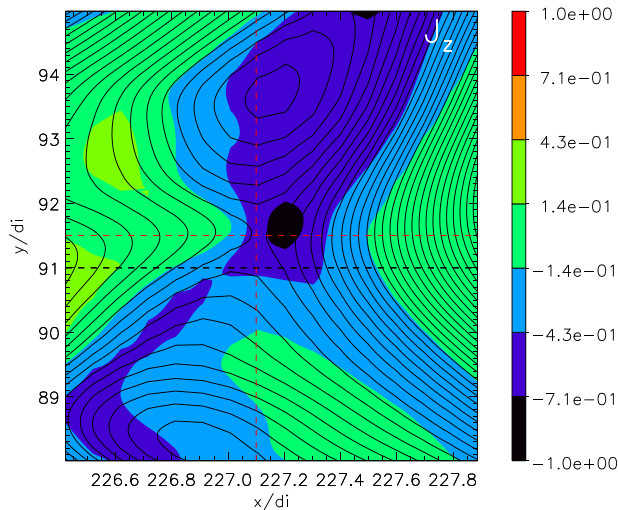


FIG. 7. Iso-contours of the out-of-plane current  $J_z$  with magnetic potential field lines (in black) for the structure in the range  $[226 - 228] d_i \times [88 - 95] d_i$ . Red dashed lines mark the position of the X-point. Virtual satellite cuts at  $y = 91 d_i$  and  $y = 92 d_i$  are marked with black dashed horizontal lines.

To provide direct evidence of reconnection, we show how different quantities vary along a virtual satellite crossing of the current sheet and we compare them with expectations for ongoing reconnection. Here we have considered the horizontal cut at  $y = 91 d_i$ , shown with black dashed line below the X-point in Fig. 7. Although the choice of the cut is arbitrary, the profiles of the different quantities do not depend significantly on the specific cut. It should be noticed that when reconnection is embedded in a turbulent background, as in our case, the typical patterns observed in simulations of magnetic reconnection initialized with one single current sheet<sup>36,37</sup> are not always easily identifiable. Nevertheless, a number of typical features of reconnection are recovered in our case. Several different quantities along the selected cut are shown in Fig. 8. All the quantities are normalized to ion characteristic parameters in the magnetosheath at the beginning of the simulation. The local reference frame of the current sheet computed through minimum variance analysis of the magnetic field is very close to the simulation frame; therefore, we use the simulation frame in our analysis.

Figure 8(a) shows the magnetic field. The reconnecting component  $B_y$  changes sign across the centre of the current sheet, while the component normal to the current sheet  $B_x$  is roughly constant and positive, as expected for a crossing of the current sheet below the X point. The out-of-plane component  $B_z$  slightly increases in the center of the current sheet,

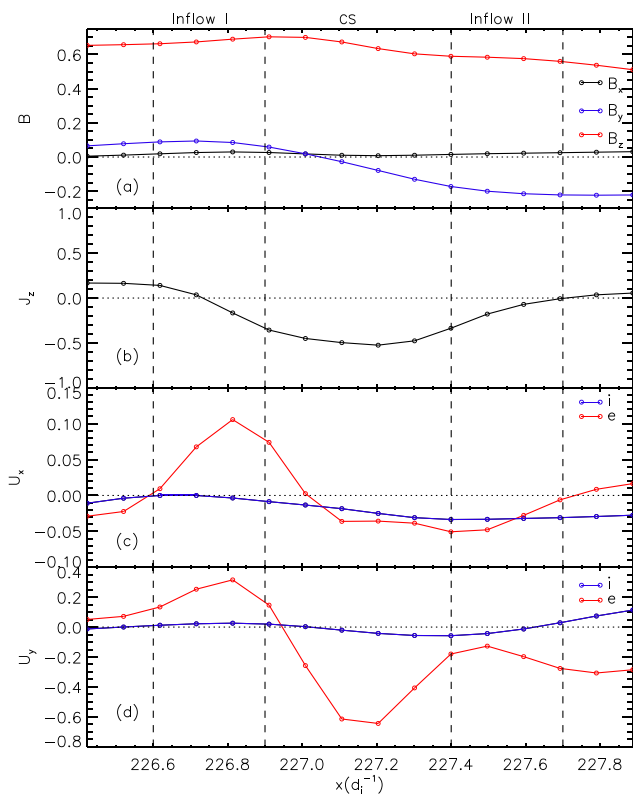


FIG. 8. (a) Components of the magnetic field  $B_x$ ,  $B_y$ , and  $B_z$ . (b) Out-of-plane current. (c) The inflow velocity  $U_x$  for both ions (red) and electrons (blue). (d) The outflow velocity  $U_y$  for both ions (in red) and electrons (in blue). Both velocity are represented in the X-point reference frame by subtracting the mean value of the ion velocity near the X-point ( $\langle U_{ix,Xpoint} \rangle = 0.24 v_A$ ,  $\langle U_{iy,Xpoint} \rangle = 0.7 v_A$ ). Vertical dashed lines indicate the two inflow regions on both sides of the current sheet and the outflow region.

as expected for Hall reconnection in case of large guide field.<sup>37</sup> It is worth to underline that around the X-points we do not observe the so-called Hall-quadrupole; a reason could be the fact that in our case, there is a large guide field ( $B_z \sim 5B_y$ ) as well as a small density asymmetry that affects the structure of the quadrupole.<sup>43,44</sup> Also note that compressibility effects could contribute to mask the presence of such Hall quadrupole.<sup>45</sup> Figure 8(b) shows the out-of-plane current  $J_z$ . The current density is slightly stronger around the left separatrix of the current sheet, as can be also observed in Fig. 7, as expected in guide field configurations.<sup>37,38</sup>

Figure 8(c) shows the ion and electron velocities normal to the current sheet  $U_{ix}$ ,  $U_{ex}$  in the X-point reference frame. This frame has been obtained by subtracting the mean ion velocity around the X-point to both ion and electron velocities. Note that such mean velocity does not change significantly when averaging over slightly different regions around the X-point. The electron velocity  $U_{ex}$  is consistent with plasma inflowing towards the center from both sides of the current sheet as expected during ongoing reconnection, being negative in the left and positive in the right inflow regions. It should be noted that the Hall regime applies everywhere, so that the inflow of plasma and of magnetic flux tubes is represented by the electron velocity since ions are unmagnetized. The value of the inflow velocity  $U_{ex}$  is consistent with fast reconnection, as discussed in detail below. Figure 8(d) shows the ion and electron outflow velocities  $U_{ey}$ ,  $U_{iy}$  in the X-point frame; we note that  $U_y < 0$ , as expected for plasmas being accelerated within the current sheet away from the X-point.

The reconnection rate was evaluated for the selected current sheet by computing the local angle between the normal,  $B_x$ , and the reconnecting,  $B_y$ , magnetic field components around the X-point, that gives the aspect ratio between the half width  $\delta$  and the half length  $L$  of the ion diffusion region.<sup>12,39</sup> We estimate this quantity by computing the ratio between the average normal magnetic field across the current sheet ( $\langle B_x \rangle$ ) and the average reconnecting component in the inflow region ( $\langle B_y \rangle$ ) as done in spacecraft data analysis.<sup>31,40,41</sup> We have found that the reconnection rate is  $R \sim 0.25$  and  $R \sim 0.1$  when averaging in the R-I and R-II inflow regions, respectively, see Table I. The difference between the values in the two regions is due to the slight asymmetry of the reconnection structure observed in this case. From the continuity equation, this aspect ratio is also the ratio between the inflow velocity  $U_x$  and the outflow velocity  $U_y$ . We therefore estimate the aspect ratio from the velocities by computing the ratio between the average electron inflow velocity ( $\langle U_{ex} \rangle$ ) and the average electron outflow velocity ( $\langle U_{ey} \rangle$ ) in the X-point frame, see Table I, and we have found  $R \sim 0.3$  and  $R \sim 0.15$  when averaging in the R-I and R-II inflow regions, respectively. The rates are normalized to the local Alfvén velocity. We also calculate the aspect ratio based on the prediction for asymmetric reconnection<sup>38</sup>  $\delta/L = [n_1 U_{x,1} + n_2 U_{x,2}] / (2n_{out} U_y)$  and found  $\delta/L \sim 0.24$ , as consistent with the fact that the asymmetries for both the density and the magnetic field are relatively small in this case. The formulas used above are valid for steady-state, non-driven reconnection where the reconnection electric field is relatively constant. In our simulation, reconnection is often unsteady and

driven by turbulent motions and therefore the rate would be higher. Yet the reconnection rate we estimate here represents a lower bound for the actual rate. The fact that we find higher rates than 0.1 even by using a steady-state assumption suggests that reconnection may be faster than we report.

A similar analysis done on several other current sheets yields similar values for the reconnection rate. The reconnection rate found for the selected current sheet is consistent with fast reconnection, even if a bit larger with respect to the rate found in simulations of single current sheet Hall reconnection with large guide field,<sup>37,42</sup> where values below 0.1 are typically recovered. One possible explanation is that when reconnection occurs in a turbulent environment, as in our case, turbulence itself can enhance the reconnection rate over the typical  $\sim 0.1$  value expected for fast reconnection, as suggested by other studies.<sup>35</sup> The turbulent dynamics may in fact act as a driver for the system, even though no external forcing is imposed. We believe that this could be one of the possible reasons for the observation of reconnection rates larger than 0.1 in our simulations.

## VI. CONCLUSIONS

In this work, we have analysed the 2D turbulence spontaneously emerging inside K-H vortices. The 2D spectral magnetic energy shows an initial anisotropy in the  $(k_x, k_y)$ -plane, due to the imposed initial velocity shear. A quantitative estimate of the anisotropy through the Shebalin angle shows an evolution towards isotropy. In the isotropic regime, a power-law spectrum  $k^{-1.8}$  has been observed above the proton inertial scale, followed by a steeper spectrum at smaller scales. Furthermore, in the saturated phase of the instability, one observes the formation of a turbulent region characterized by the presence of small scale fluctuations and structures of the order of one inertial length or less.

We have observed a scale dependent deviation from Gaussianity of the magnetic field increments, as consistent with the generation of intense small scale fluctuations and structures, typical of intermittent turbulence. Our results are in agreement with previous results from PIC simulations of shear flow turbulence.<sup>5,6,26</sup>

A detailed analysis of such intense structures on scales of the order of the proton inertial length, identified with the PVI method,<sup>29,30</sup> shows that they are consistent with reconnecting current sheets. A reconnection rate  $R \simeq 0.1\text{--}0.3$  has been found, slightly larger than the typical Hall reconnection rate for a single current sheet with guide field<sup>37,42</sup> but in agreement with other simulations of reconnection in a turbulent medium.<sup>35</sup>

The study of the reconnection regions performed in a way similar to *in-situ* satellite data analysis<sup>31,41</sup> extends based on the analysis of the magnetic field topology.<sup>30,35</sup> Yet, the complex structure of the magnetic field and plasma around the current sheets often makes a clear identification of the inflow/outflow regions difficult, so that a statistical analysis is not straightforward. Nevertheless, a number of significant features of intermittency and reconnecting current sheets have been pointed out in our simulations. All this can be used to guide the analysis of turbulent reconnection

within K-H vortices with data from recent and future spacecraft missions, in particular, the NASA/MMS mission which is tailored to study the microphysics of reconnection and ESA/THOR, a mission concept currently under study phase and fully devoted to study energy dissipation and particle energization in turbulent plasmas. Improved diagnostic of reconnection sites in turbulence simulations in the coming future would therefore be advantageous.

Our finding that thin reconnecting current sheets form in K-H turbulence supports reconnection as a fundamental dissipation mechanism in turbulent plasmas, as recently proposed by several authors.<sup>5,6,31–33,35,46</sup>

## ACKNOWLEDGMENTS

The research leading to these results has received funding from the European Commissions Seventh Framework Programme (FP7/2007-2013) under the Grant Agreements: 263340/SWIFF ([www.swiff.eu](http://www.swiff.eu)) and 269279/TURBOPLASMAS.

We acknowledge the access to SuperMUC machine at LRZ made available within the PRACE initiative receiving funding from the European Commissions Seventh Framework Programme (FP7/2007-2013) under Grant Agreement No. RI-283493 and Project No. 2012071282. The authors gratefully acknowledge the Gauss Centre for Supercomputing e.V. ([www.gauss-centre.eu](http://www.gauss-centre.eu)) for funding this project by providing computing time on the GCS Supercomputer SuperMUC at Leibniz Supercomputing Centre (LRZ, [www.lrz.de](http://www.lrz.de)).

We acknowledge ISSI Team 292 “Kinetic Turbulence and Heating in the Solar Wind.” Finally, L.S.V. acknowledges the Italian CNR Short Term Mobility Program 2014.

<sup>1</sup>M. N. Izakov, *Sol. Syst. Res.* **41**, 355 (2007).

<sup>2</sup>G. Zimbardo, A. Greco, P. Veltri, Z. Voros, and A. Taktakishvili, *Astrophys. Space Sci. Trans.* **4**, 35 (2008).

<sup>3</sup>R. Bruno and V. Carbone, *Living Rev. Sol. Phys.* **2**, 4 (published online 2005).

<sup>4</sup>J. E. Borovsky and H. O. Funsten, *J. Geophys. Res.: Space Phys.* **108**(A7), 1284, doi:10.1029/2002JA009625 (2003).

<sup>5</sup>M. Wan, W. Matthaeus, H. Karimabadi, V. Roytershteyn, M. Shay, P. Wu, W. Daughton, B. Loring, and S. C. Chapman, *Phys. Rev. Lett.* **109**, 195001 (2012).

<sup>6</sup>H. Karimabadi, V. Roytershteyn, M. Wan, W. Matthaeus, W. Daughton, P. Wu, M. Shay, B. Loring, J. Borovsky, E. Leonardi *et al.*, *Phys. Plasmas* **20**, 012303 (2013).

<sup>7</sup>H. Hasegawa, *Monogr. Environ. Earth Planets* **1**, 71 (2012).

<sup>8</sup>A. Miura, *J. Geophys. Res.: Space Phys.* **89**, 801, doi:10.1029/JA089iA02p00801 (1984).

<sup>9</sup>H. Hasegawa, M. Fujimoto, T.-D. Phan, H. Rème, A. Balogh, M. Dunlop, C. Hashimoto, and R. TanDokoro, *Nature* **430**, 755 (2004).

<sup>10</sup>S. Servidio, V. Carbone, L. Primavera, P. Veltri, and K. Stasiewicz, *Planet. Space Sci.* **55**, 2239 (2007).

<sup>11</sup>K. Nykyri and A. Otto, *Geophys. Res. Lett.* **28**, 3565, doi:10.1029/2001GL013239 (2001).

<sup>12</sup>M. Faganello, F. Califano, and F. Pegoraro, *Phys. Rev. Lett.* **100**, 015001 (2008).

<sup>13</sup>S. Wing and P. T. Newell, *Geophys. Res. Lett.* **29**, 1307, doi:10.1029/2001GL013950 (2002).

<sup>14</sup>H. Hasegawa, M. Fujimoto, K. Takagi, Y. Saito, T. Mukai, and H. Rème, *J. Geophys. Res.: Space Phys.* **111**, A09203 (2006).

<sup>15</sup>M. Faganello, F. Califano, and F. Pegoraro, *N. J. Phys.* **11**, 063008 (2009).

<sup>16</sup>P. Henri, S. Cerri, F. Califano, F. Pegoraro, C. Rossi, M. Faganello, O. Šebek, P. Trávníček, P. Hellinger, J. Frederiksen *et al.*, *Phys. Plasmas* **20**, 102118 (2013).

<sup>17</sup>S. K. Lele, *J. Comput. Phys.* **103**, 16 (1992).

- <sup>18</sup>J. V. Shebalin, W. H. Matthaeus, and D. Montgomery, *J. Plasma Phys.* **29**, 525 (1983).
- <sup>19</sup>G. Zimbardo, A. Greco, L. Sorriso-Valvo, S. Perri, Z. Vörös, G. Aburjania, K. Chargazia, and O. Alexandrova, *Space Sci. Rev.* **156**, 89 (2010).
- <sup>20</sup>O. Alexandrova, C. H. K. Chen, L. Sorriso-Valvo, T. S. Horbury, and S. D. Bale, *Space Sci. Rev.* **178**, 101 (2013).
- <sup>21</sup>L. Rezeau, *Acad. Sci. Paris C. R. Ser. II B Sci. Phys.* **327**, 299 (1999).
- <sup>22</sup>F. Sahraoui, G. Belmont, L. Rezeau, N. Cornilleau-Wehrlin, J. Pinçon, and A. Balogh, *Phys. Rev. Lett.* **96**, 075002 (2006).
- <sup>23</sup>U. Frisch, *Turbulence: The Legacy of AN Kolmogorov* (Cambridge University Press, 1995).
- <sup>24</sup>R. Bruno and V. Carbone, *Living Rev. Sol. Phys.* **2**, 4 (published online 2005).
- <sup>25</sup>L. Sorriso-Valvo, V. Carbone, P. Veltri, G. Consolini, and R. Bruno, *Geophys. Res. Lett.* **26**, 1801, doi:10.1029/1999GL900270 (1999).
- <sup>26</sup>E. Leonardis, S. C. Chapman, W. Daughton, V. Roytershteyn, and H. Karimabadi, *Phys. Rev. Lett.* **110**, 205002 (2013).
- <sup>27</sup>K. R. Sreenivasan and R. Antonia, *Annu. Rev. Fluid Mech.* **29**, 435 (1997).
- <sup>28</sup>F. Anselmet, Y. Gagne, E. Hopfinger, and R. Antonia, *J. Fluid Mech.* **140**, 63 (1984).
- <sup>29</sup>A. Greco, P. Chuychai, W. Matthaeus, S. Servidio, and P. Dmitruk, *Geophys. Res. Lett.* **35**, L19111, doi:10.1029/2008GL035454 (2008).
- <sup>30</sup>S. Servidio, A. Greco, W. Matthaeus, K. Osman, and P. Dmitruk, *J. Geophys. Res.: Space Phys.* **116**, A09102, doi:10.1029/2011JA016569 (2011).
- <sup>31</sup>A. Retinò, D. Sundkvist, A. Vaivads, F. Mozer, M. André, and C. Owen, *Nat. Phys.* **3**, 236 (2007).
- <sup>32</sup>D. Sundkvist, A. Retinò, A. Vaivads, and S. D. Bale, *Phys. Rev. Lett.* **99**, 025004 (2007).
- <sup>33</sup>A. Chasapis, A. Retinò, F. Sahraoui, A. Vaivads, Y. V. Khotyaintsev, D. Sundkvist, A. Greco, L. Sorriso-Valvo, and P. Canu, *Astrophys. J. Lett.* **804**, L1 (2015).
- <sup>34</sup>K. Osman, W. Matthaeus, J. Gosling, A. Greco, S. Servidio, B. Hnat, S. C. Chapman, and T. Phan, *Phys. Rev. Lett.* **112**, 215002 (2014).
- <sup>35</sup>S. Servidio, W. Matthaeus, M. Shay, P. Cassak, and P. Dmitruk, *Phys. Rev. Lett.* **102**, 115003 (2009).
- <sup>36</sup>P. Pritchett, *J. Geophys. Res.: Space Phys.* **106**, 3783 (2001).
- <sup>37</sup>P. Pritchett and F. Coroniti, *J. Geophys. Res.: Space Phys.* **109**, A01220, doi:10.1029/2003JA009999 (2004).
- <sup>38</sup>P. Cassak and M. Shay, *Phys. Plasmas* **14**, 102114 (2007).
- <sup>39</sup>P. Henri, F. Califano, M. Faganello, and F. Pegoraro, *Phys. Plasmas* **19**, 072908 (2012).
- <sup>40</sup>A. Vaivads, Y. Khotyaintsev, M. André, A. Retino, S. Buchert, B. Rogers, P. Décréau, G. Paschmann, and T. Phan, *Phys. Rev. Lett.* **93**, 105001 (2004).
- <sup>41</sup>H. Hasegawa, A. Retinò, A. Vaivads, Y. Khotyaintsev, M. André, T. Nakamura, W.-L. Teh, B. Sonnerup, S. Schwartz, Y. Seki *et al.*, *J. Geophys. Res.: Space Phys.* **114**, A12207, doi:10.1029/2009JA014042 (2009).
- <sup>42</sup>J. Huba and L. Rudakov, *Phys. Rev. Lett.* **93**, 175003 (2004).
- <sup>43</sup>M. Swisdak, J. Drake, M. Shay, and J. McIlhargey, *J. Geophys. Res.: Space Phys.* **110**, A05210, doi:10.1029/2004JA010748 (2005).
- <sup>44</sup>P. Pritchett, *J. Geophys. Res.: Space Phys.* **113**, A06210, doi:10.1029/2007JA012930 (2008).
- <sup>45</sup>M. Faganello, F. Califano, and F. Pegoraro, *Phys. Rev. Lett.* **101**, 105001 (2008).
- <sup>46</sup>M. Wan, W. Matthaeus, V. Roytershteyn, H. Karimabadi, T. Parashar, P. Wu, and M. Shay, *Phys. Rev. Lett.* **114**, 175002 (2015).